

Gradient-Based Aperiodic Array Synthesis of Real Arrays With Uniform Amplitude Excitation Including Mutual Coupling

J. Ignacio Echeveste, Miguel Á. González de Aza, Jesús Rubio, and Christophe Craeye, *Senior Member, IEEE*

Abstract—This paper proposes the synthesis of aperiodic arrays of realistic antennas excited with uniform amplitude, where the mutual coupling between elements is rigorously taken into account. A cost function that involves the expression of the radiated field of the coupled array is obtained and its gradient is evaluated in order to move the elements in the corresponding direction at each iteration. The synthesis method involves the calculation of the gradient of the field radiated by the coupled array, which is obtained analytically by using a full-wave method based on the generalized scattering matrix, spherical mode expansions and rotation, and translation properties of spherical waves.

Index Terms—Aperiodic arrays, array synthesis, gradient method, local optimization, mutual coupling, spherical waves.

I. INTRODUCTION

ALTHOUGH sparse or aperiodic arrays were first studied more than four decades ago [1], they recently demonstrated to represent a promising and a challenging technology for different kinds of applications, such as low-frequency radio telescopes [2], [3], satellite communications [4], or SAR observations [5]. Sparse array antennas are adequate for large aperture radio telescopes because they are required to work in an ultrawide frequency band. In order to avoid an oversampled array at the lower frequencies, the array has to be sparse at the upper ones [6]. Two main drawbacks appear when a phased array is considered: really high cost due to the high number of elements and the poor efficiency induced by the amplitude tapering. Using sparse arrays, the number of elements, and consequently the number of control points, can be drastically reduced, thereby decreasing the cost of conventional

phased arrays. With a uniform amplitude excitation, allowing a phase variation to steer the beam, the second drawback is also avoided because every amplifier works at its optimal level.

Sparse arrays also have some drawbacks compared with regular array distributions. The number of elements can be reduced without modifying the beamwidth but the aperture efficiency is going to be poorer than the one of a regular array fully populated and uniformly excited, independently of the design process. There are some approaches to mitigate this effect such as designing elements of different sizes [7] or interleaved subarrays [8]. Another difficulty arises from the designer point of view: the complexity grows. Some approaches used in the analysis of equispaced arrays, as imposing periodic boundaries, cannot be used here, and a large full-wave analysis may be needed in order to obtain an accurate characterization of the radiating structure. Rigorous and efficient analysis methods that can be employed for large and sparse arrays have been proposed over the last decade. Some of them are based on macro basis function [9], [10], where a reduction in the number of unknowns is accomplished with a negligible error. Another approach was presented in [11] where the elements are enclosed in spheres or hemispheres, while the field radiated by each element is expressed as an expansion of spherical waves. In that way, the elements can be individually analyzed in presence of mutual coupling obtaining a much smaller system of equations.

The optimization of aperiodic arrays induces also a more complex problem from the synthesis point of view, due to the sparse distribution of the problem. Indeed, most of the classical synthesis methods usually applied to periodic arrays [12], [13], cannot be applied here. In an equispaced or periodic array, the degrees of freedom are the excitation weights which have a linear behavior and for which optimal solutions can be found efficiently, for instance, using convex optimization [14]. However, sparse arrays, where the location of the elements are the variables of the problem, have a highly nonconvex behavior which causes an NP-hard problem that is difficult to deal with [15]. Nonuniformly excited sparse arrays can accomplish very stringent specifications but the reduction in the cost is not as big as when the elements are uniformly excited, and they still suffer from poor aperture efficiency due to the amplitude variation. Thinned arrays can reduce the number of elements but they may suffer from drawbacks

Manuscript received December 9, 2015; revised June 26, 2016; accepted November 16, 2016. Date of publication December 9, 2016; date of current version February 1, 2017. This work was supported in part by MINECO Spain, under Contract TEC2013-46282-C2-1-P and Contract TEC2013-46282-C2-2P and in part by FEDER (EU).

J. Ignacio Echeveste and C. Craeye are with the ICTTEAM Institute, Université catholique de Louvain, 1348 Louvain-la-Neuve, Belgium (e-mail: jose.echeveste@uclouvain.be; christophe.craeye@uclouvain.be).

M. A. González de Aza is with the Departamento de Señales, Sistemas y Radiocomunicaciones, E.T.S.I. Telecomunicación, Universidad Politécnica de Madrid, Ciudad Universitaria, 28040 Madrid, Spain (e-mail: mag@etc.upm.es).

J. Rubio is with the Dpto. de Tecnología de Computadores y Comunicaciones, Escuela Politécnica de Cáceres, Universidad de Extremadura, 10071 Cáceres, Spain (e-mail: jesusrubio@unex.es).

Color versions of one or more of the figures in this paper are available online at <http://ieeexplore.ieee.org>.

Digital Object Identifier 10.1109/TAP.2016.2638359

associated with periodic distributions if the thinning is not very strong. Here, we will focus on uniformly excited sparse arrays. Several methods are available in the literature for synthesizing aperiodic, sparse, or thinned arrays. Some of these methods are based on global and computationally intensive approaches such as in [16], and some others are based on density tapering techniques proposed in [17], as [18]. On the other hand, in most of these methods, the mutual coupling and the full wave analysis of realistic elements are not considered, because it is not easy to merge an electromagnetic analysis into an array synthesis process. In some other works, it is argued that as the elements are placed in a sparse grid, the mutual coupling is not significant and can be avoided [18] which we will show it is only partially true.

The analysis methods mentioned earlier deal with fixed positions and the synthesis techniques often consider the elements as isotropic sources. Other array synthesis methods account for mutual coupling but with fixed positions. A synthesis method is presented in [19] where the authors proposed a sparse array synthesis that can incorporate the mutual coupling represented with an impedance matrix, based on the work presented in [20]. But as commented in the latter reference, this kind of simplification is valid only for certain kinds of antennas that can be cast as minimum-scattering antennas. In [21], the mutual coupling effect is computed after the synthesis in order to evaluate its importance, but it is not part of the optimization process. Reference [22] presents a method for sparse arrays where a convex problem is solved iteratively in order to get some desired specification with the minimum number of elements. In [23], the positions of the elements of an aperiodic array, uniformly excited in amplitude, are synthesized solving iteratively convex problems as well. In both papers, the elements are considered to be isolated and mutual coupling is not accounted for. In [24], a similar iterative procedure is exploited, where at each iteration, the mutual coupling of a linear array is computed but is not taken into account when deciding the direction in which the elements should be moved.

In this paper, we propose a local optimization procedure for the synthesis of aperiodic arrays, based on the gradient algorithm presented in [25] for isotropic sources, and on the analysis method presented in [11]. The analysis method is based on a description of the radiated field as an expansion of spherical waves. The array elements are characterized from a full-wave analysis technique and the mutual coupling between them is rigorously taken into account. In [25], the gradient method is part of a three steps algorithm. At each iteration, a cost function involving the array factor is obtained and its gradient with respect to the coordinates of the elements is computed. According to the result of the gradient, the elements are moved, over a desired distance, in the appropriate direction, checking at each movement that the elements do not overlap and that the area covered by the array satisfies the imposed limits. As the method is local and the problem is not convex, the solutions obtained will not be claimed to be the global solutions of the problem, since this solution will depend on the initial array configuration. Taking this into account, different starting positions will be considered in order to provide the

best possible solutions. To the authors' best knowledge, this is the first time that a power synthesis method is presented for sparse arrays with uniform amplitude excitation, in which the mutual coupling is rigorously included in the computation of the gradient of the cost function, and consequently in the decision process.

This paper is divided as follows. In Section II, the analysis method used to obtain a closed-form expression for the radiated field of the coupled array is recalled. In Section III, the synthesis method is detailed. It is composed of two steps. The first one consists of the starting point, obtained for instance with a density taper and the second one is the local gradient-based method. Some results for linear and planar arrays of realistic volumetric elements will be shown in Section IV. The conclusions are presented in Section V.

II. GSM REPRESENTATION OF AN ARRAY OF COUPLED ANTENNAS

In this section, the validated analysis method of coupled antennas arrays developed in [11], and integrated in the synthesis methodology proposed in this paper, is briefly summarized. This method provides a rigorous characterization of antenna arrays whose elements can be described by means of spherical waves, such as planar arrays on an infinite ground plane. The analysis methodology consists of two processes. In the first one, each element of the array, considered as isolated, is characterized by a full-wave and modular procedure based on the 3-D finite element method (FEM), a modal analysis and a domain decomposition technique [26]. A modal expansion is used on the feeding ports and a spherical mode expansion on a hemisphere surface (spherical port) is used to characterize the radiating region. The analysis provides for each antenna of the array a generalized scattering matrix (GSM) that relates the coefficients of the modal expansions in these ports

$$\begin{bmatrix} \Gamma_i & R_i \\ T_i & S_i - I_i \end{bmatrix} \begin{bmatrix} v_i \\ a_i \end{bmatrix} = \begin{bmatrix} w_i \\ b_i \end{bmatrix} \quad (1)$$

v_i , w_i , a_i , and b_i are column vectors containing, respectively, the complex amplitudes of incident and reflected modes on the feeding ports, and the incoming and scattered spherical modes on the spherical ports. The submatrices Γ_i , R_i , T_i , and S_i are, respectively, the individual reflection, reception, transmission, and scattering matrices of the antenna i , and I_i is the identity matrix.

In the following step of the analysis method, the overall GSM of the coupled finite array is analytically computed from GSMs of the single elements by applying properties of rotation and translation of spherical waves. If an antenna array with N elements is considered, and if it is first assumed that the array elements are uncoupled, the whole array would be characterized by means a GSM as follows:

$$\begin{bmatrix} \Gamma & R \\ T & S - I \end{bmatrix} \begin{bmatrix} v \\ a \end{bmatrix} = \begin{bmatrix} w \\ b \end{bmatrix} \quad (2)$$

where $\mathbf{\Gamma}$ is a diagonal block-matrix defined by $\mathbf{\Gamma} = \text{diag}(\mathbf{\Gamma}_i)$, and the same applies for \mathbf{R} , \mathbf{T} , and $(\mathbf{S} - \mathbf{I})$, and

$$\mathbf{v} = \begin{bmatrix} v_1 \\ \vdots \\ v_N \end{bmatrix} \quad \mathbf{w} = \begin{bmatrix} w_1 \\ \vdots \\ w_N \end{bmatrix}$$

$$\mathbf{a} = \begin{bmatrix} a_1 \\ \vdots \\ a_N \end{bmatrix} \quad \mathbf{b} = \begin{bmatrix} b_1 \\ \vdots \\ b_N \end{bmatrix}. \quad (3)$$

In order to account for mutual coupling, the incident field on each antenna of the array is now considered as the superposition of the field coming from outside the array and the field scattered by the remaining elements of the array. In this way, if each one of these fields is expanded into spherical modes, the complex amplitudes of the incoming modes in element i , \mathbf{a}_i are obtained as

$$\mathbf{a}_i = \mathbf{a}_{di} + \sum_{\substack{j=1 \\ j \neq i}}^N \mathbf{a}_i^j \quad (4)$$

where \mathbf{a}_{di} and \mathbf{a}_i^j are, respectively, column vectors containing incoming modes from outside the array in element i , and \mathbf{a}_i^j scattered modes from the element j translated to the position of element i . Each one of the column vectors \mathbf{a}_i^j is then related to the scattered spherical mode coefficients in the antenna j by means of the following relation, as shown in [27]:

$$\mathbf{a}_i^j = \mathbf{G}_{ij} \mathbf{b}_j. \quad (5)$$

\mathbf{G}_{ij} is the general translation matrix between antennas i and j obtained by using rotation and translation properties of spherical waves. This matrix includes in the most general case, rotations, axial translation, and inverse rotations of spherical waves [11]. By substituting (5) into (4) for each radiating element, the incoming modes for all the antennas of the array is obtained

$$\mathbf{a} = \mathbf{a}_d + \mathbf{G}\mathbf{b} \quad (6)$$

where \mathbf{a}_d is given by

$$\mathbf{a}_d = (\mathbf{a}_{d1}^T \dots \mathbf{a}_{di}^T \dots \mathbf{a}_{dN}^T)^T \quad (7)$$

and \mathbf{G} is a square matrix obtained from elements \mathbf{G}_{ij} as follows:

$$\mathbf{G} = \begin{bmatrix} 0 & \mathbf{G}_{12} & \dots & \dots & \mathbf{G}_{1N} \\ \mathbf{G}_{21} & 0 & \ddots & \mathbf{G}_{ij} & \dots \\ \dots & \ddots & \ddots & \ddots & \dots \\ \dots & \mathbf{G}_{ji} & \ddots & 0 & \mathbf{G}_{N-1N} \\ \mathbf{G}_{N1} & \dots & \dots & \mathbf{G}_{NN-1} & 0 \end{bmatrix}. \quad (8)$$

Finally, the overall GSM of the finite array including mutual coupling between elements is defined as

$$\begin{bmatrix} \mathbf{\Gamma}_G & \mathbf{R}_G \\ \mathbf{T}_G & \mathbf{S}_G - \mathbf{I}_G \end{bmatrix} \begin{bmatrix} \mathbf{v} \\ \mathbf{a}_d \end{bmatrix} = \begin{bmatrix} \mathbf{w} \\ \mathbf{b} \end{bmatrix}. \quad (9)$$

It is obtained by substituting (6) into (2) after matrix operations. The submatrices $\mathbf{\Gamma}_G$, \mathbf{R}_G , \mathbf{T}_G , and \mathbf{S}_G , stand, respectively, for the reflection coefficient, reception, transmission, and scattering matrices of the finite array and are given by

$$\begin{aligned} \mathbf{\Gamma}_G &= \mathbf{\Gamma} + \mathbf{R}\mathbf{G}[\mathbf{I} - (\mathbf{S} - \mathbf{I})\mathbf{G}]^{-1}\mathbf{T} \\ \mathbf{R}_G &= \mathbf{R} + \mathbf{R}\mathbf{G}[\mathbf{I} - (\mathbf{S} - \mathbf{I})\mathbf{G}]^{-1}(\mathbf{S} - \mathbf{I}) \\ \mathbf{T}_G &= [\mathbf{I} - (\mathbf{S} - \mathbf{I})\mathbf{G}]^{-1}\mathbf{T} \\ (\mathbf{S}_G - \mathbf{I}_G) &= [\mathbf{I} - (\mathbf{S} - \mathbf{I})\mathbf{G}]^{-1}(\mathbf{S} - \mathbf{I}). \end{aligned} \quad (10)$$

Therefore, a closed-form GSM which rigorously describes the array as a circuit is obtained providing the impedance, coupling, radiating, and scattering characteristics of the array for any arbitrary excitation. The method is valid for arrays with different elements, placed in arbitrary positions and with complex geometries, since they are characterized using the FEM.

The radiated far field of an array for a desired excitation \mathbf{v} will be obtained as an expansion of spherical modes weighted by complex coefficients \mathbf{b} . In this way, considering a planar array of N antennas placed in the xy plane, and M spherical modes for each antenna, and denoted by $\mathbf{e}_m(\theta, \phi)$ the electric field corresponding to the m th spherical mode on each antenna, and by b_{im} the coefficient corresponding to this mode on the antenna i , the radiated field is expressed as

$$\mathbf{E}(\hat{u}) = \sum_{i=1}^N \mathbf{e}(\hat{u}) \mathbf{b}_i e^{jk\hat{u} \cdot \mathbf{u}_i} \quad (11)$$

where $\mathbf{e}(\hat{u})$ is a row vector given by $\mathbf{e} = (\mathbf{e}_1, \mathbf{e}_2, \dots, \mathbf{e}_m)$, \mathbf{b}_i is a column vector defined by $\mathbf{b}_i = (b_{i1}, b_{i2}, \dots, b_{im})^T$, the variable k is the wavenumber in free space, the vector \hat{u} refers to the unitary vector in spherical coordinates $\hat{u} = (u_x, u_y, u_z)$ and the vector $\mathbf{u}_i = x_i\hat{x} + y_i\hat{y}$ is the position vector of the antenna i . Developing the summation in (11) yields

$$\mathbf{E}(\hat{u}) = (\mathbf{e} e^{jk\hat{u} \cdot \mathbf{u}}) \mathbf{b} \quad (12)$$

where

$$(\mathbf{e} e^{jk\hat{u} \cdot \mathbf{u}}) = (\mathbf{e} e^{jk\hat{u} \cdot \mathbf{u}_1} \quad \mathbf{e} e^{jk\hat{u} \cdot \mathbf{u}_2} \dots \mathbf{e} e^{jk\hat{u} \cdot \mathbf{u}_N}) \quad (13)$$

and \mathbf{b} is the column vector containing the vectors \mathbf{b}_i . Assuming that there is no incident field from the exterior, $\mathbf{a}_d = 0$ in (9), the coefficients \mathbf{b} are obtained from the transmission matrix applying a desired excitation, $\mathbf{b} = \mathbf{T}_G \mathbf{v}$, where, without loss of generality, a single excitation mode in each feeding port is considered $\mathbf{v} = (v_1, v_2, \dots, v_N)^T$. Substituting \mathbf{b} into (12) results in

$$\mathbf{E}(\hat{u}) = (\mathbf{e}(\hat{u}) e^{jk\hat{u} \cdot \mathbf{u}}) \mathbf{T}_G \mathbf{v}. \quad (14)$$

This expression provides the field radiated by the coupled array in a rigorous way and will be used in the synthesis method.

III. PROPOSED SYNTHESIS METHOD

In this section, the synthesis method is detailed. A cost function that involves the radiation intensity of the coupled array is obtained, a weighting function depending on the direction is computed and analytical expressions are obtained

for the gradient of the cost function with respect to element positions.

A. Cost Function, Constraints, and Optimization Procedure

The optimization method looks for the synthesis of the radiation pattern of antenna arrays, while accounting for realistic radiating elements as well as the mutual coupling between them. The elements distribution in the nonregular array that minimizes the sidelobe level (SLL), while fixing a mainbeam with a fixed width, is optimized. The excitation amplitudes are assumed constant. The secondary lobes are minimized via a cost function that involves an average of the sidelobes, through weighting by a desired function. The local method proposed here iteratively moves a given number of elements in a defined area (circular for the planar array), while fixing a minimum distance between elements in order to avoid overlapping. The elements are uniformly excited in amplitude, and a linear phase distribution can be imposed in order to steer the beam.

As proposed in [25], instead of looking for minimizing exclusively the maximum SLL, the minimization of a certain type of average measure of the SLL is considered. The cost function is obtained by averaging the radiation intensity and using a weighting function, $W(\hat{u})$, to focus on selected regions. In this way, the cost function to be minimized is defined as

$$CF = \left(\int_U [W(\hat{u})|E(\hat{u})|^2]^p d\hat{u} \right)^{1/p} \quad (15)$$

where U is the desired integration region in which the SLL has to be minimized and p stands for the exponent that characterizes the L_p -norm. A low value for p is used when an average of the SLL is desired while a higher value will make more emphasis on peaks of the radiated intensity in the sidelobe region.

The cost function for the coupled antenna array is obtained by substituting in (15) the radiation intensity of the coupled antenna array which is obtained directly from the expression of the radiated field (14) as

$$\begin{aligned} |E(\hat{u})|^2 &= |(e(\hat{u}) e^{jk\hat{u}\cdot\mathbf{u}}) \mathbf{T}_G \mathbf{v}|^2 \\ &= \mathbf{v}^H \mathbf{T}_G^H (e(\hat{u}) e^{jk\hat{u}\cdot\mathbf{u}})^H \cdot (e(\hat{u}) e^{jk\hat{u}\cdot\mathbf{u}}) \mathbf{T}_G \mathbf{v} \\ &= \mathbf{v}^H \mathbf{P} \mathbf{v} \end{aligned} \quad (16)$$

where the superscript H stands for the Hermitian transpose and

$$\mathbf{P} = \mathbf{T}_G^H (e(\hat{u}) e^{jk\hat{u}\cdot\mathbf{u}})^H \cdot (e(\hat{u}) e^{jk\hat{u}\cdot\mathbf{u}}) \mathbf{T}_G \quad (17)$$

has been defined.

Finally, the cost function reads

$$CF = \left(\int_U [W(\hat{u})(\mathbf{v}^H \mathbf{P} \mathbf{v})]^p d\hat{u} \right)^{1/p}. \quad (18)$$

This expression enables an analytical differentiation with respect to the array-elements positions in such a way that the gradient-based local optimization method proposed in [25] for isotropic elements will be applicable for realistic and coupled array elements. As shown in [25], the first step of the optimization process consists of the computation of the global gradient of the cost function with respect to the coordinates

of every antenna of the array. The elements are then moved iteratively in the direction opposite to its corresponding partial gradient, along a distance obtained as the multiplication of the gradient by a constant step δ . A larger δ will require fewer iterations to obtain the solution, but if it is too large the convergence can be modified. A minimum distance between elements is selected in order to make the array physically realizable and a maximum allowable distance with respect to the array center is selected. In every movement, these constraints are verified by checking that the elements do not overlap and do not get out of the dimension limits. If any of those happens, the elements are still moved following the direction obtained from the gradient computation, up to the limit associated with the minimum-distance constraints.

B. Weighting Functions and Initial Distribution

The local method proposed here depends on the initial distribution of the array elements and the selected weighting function. A good starting point and a proper weighting function will lead to better results or will require fewer iterations. Different initial distributions can be considered, as for example the sunflower distribution proposed in [28], those obtained with the classical method proposed in [17], with the gradient-based method for isotropic sources proposed in [25] or just a random or a regular distribution. The beamwidth of an array is generally insensitive to the distribution and to the number of elements. It directly depends on the aperture length of the array, defined by the two most distant elements of the array. A small beamwidth can be obtained with a small number of elements if they are placed nonuniformly, but the secondary lobes will increase if the distance between elements grows. For an equispaced array, the highest secondary lobes are usually placed close to the main beam, which is not the case for nonuniformly distributed arrays, especially when they are sparse.

The utilization of the weighting function $W(\hat{u})$ provides more degrees of freedom to the designer because, depending on the desired radiation pattern and on the initial distribution, more importance can be given to specific ranges of directions. $W(\hat{u})$ has to be selected wisely in order to minimize the radiated field in desired regions. Some prior knowledge can be applied to the weighting function if the number of elements and the maximum allowed size of the array is known in advance. If the starting point of the synthesis is a uniform distribution and the objective is to minimize the highest secondary lobe level, a weighting function that emphasizes lobes near the mainlobe would be the most adequate. In Fig. 1, different weighting functions used in this paper are represented. If a sparse distribution is employed as an initial distribution, depending on the distance between elements, the highest secondary lobes will appear in different directions. For example, if the density method presented in [17] is selected to distribute the elements, the following study may be useful to know in advance where the highest secondary lobes are situated. As a proof of concept, the example of a linear array of isotropic sources with a total length of $20\lambda_0$ is considered. Different array configurations can be designed by varying the number of elements, and consequently the average

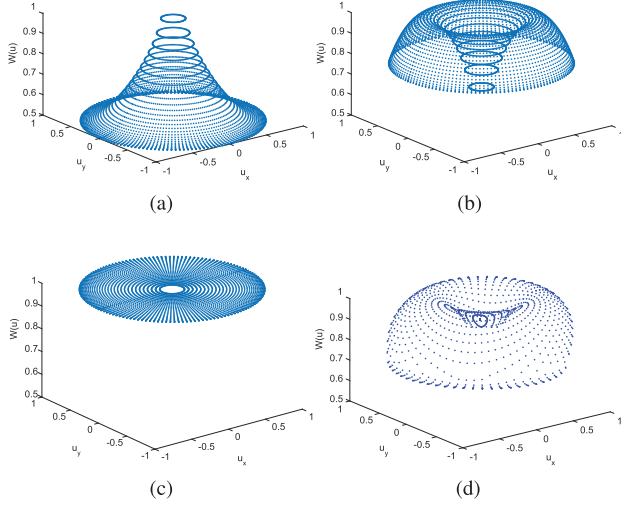


Fig. 1. Different weighting functions used in this paper.

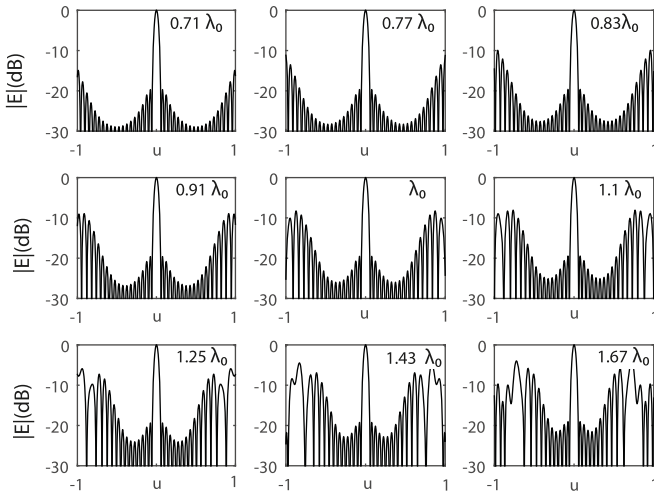


Fig. 2. Radiated field and the appearance of secondary lobes for using an array of isotropic elements placed with the initial distribution obtained with the density synthesis presented in [17]. The study is performed for a fixed array length ($20\lambda_0$) and varying the average distance between elements, $0.71 - 1.67\lambda_0$ (indicated in the graphics), and consequently the number of elements, $28 - 12$.

distance between elements varies. Fig. 2 shows the results from the density synthesis of linear arrays with an average distance between 0.71 and 1.67 wavelengths, corresponding to 28 to 12 elements. In examples with a low number of elements, it can be observed that the secondary lobes are higher in the *noncoherent region* [25]. Depending on the average distance between elements, these secondary lobes appear for smaller or bigger angles while the beamwidth of the main lobe is not modified. Taking this into account, different weighting functions will be chosen in order to focus on different regions, depending on the starting configuration. Similar procedures can be followed for the different starting points.

C. Gradient of the Cost Function of the Coupled Array

The cost function was defined in (15) in terms of the positions of the elements in the array. Next, the gradient of the cost function with respect to the coordinates of every antenna (x for a linear array, x and y for a planar array) is computed

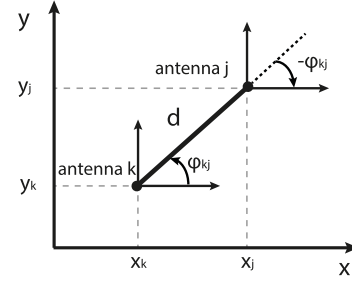


Fig. 3. Coordinates of antennas j and k separated a distance d and definition of the angle ϕ_{kj} .

as follows:

$$\frac{\partial CF}{\partial x_i} = (CF)^{1-p} \int_u W(\hat{u})^p [v^H P v]^{p-1} \frac{\partial (v^H P v)}{\partial x_i} d\hat{u}. \quad (19)$$

The derivative of the radiation intensity in (19), is computed by substituting (17) and reads

$$\begin{aligned} \frac{\partial |E(\hat{u})|^2}{\partial x_i} &= v^H \frac{\partial P}{\partial x_i} v \\ &= v^H \frac{\partial [\mathbf{T}_G^H(e(\hat{u}) e^{jk\hat{u}\cdot u})^H \cdot (e(\hat{u}) e^{jk\hat{u}\cdot u}) \mathbf{T}_G]}{\partial x_i} v. \end{aligned} \quad (20)$$

This expression is computed applying the properties of the derivatives of products and taking into account the factors in P that depend on the positions. Two derivatives are computed separately. On the one hand, the term that relates the exponential function and the spherical modes is derived as

$$\frac{\partial (e(\hat{u}) e^{jk\hat{u}\cdot u})}{\partial x_i} = jk(e(\hat{u}) e^{jk\hat{u}\cdot u}) \frac{\partial (\hat{u} \cdot u)}{\partial x_i}. \quad (21)$$

On the other hand, the transmission matrix of the finite array, \mathbf{T}_G , which has been previously defined in (10), can be rewritten for simplicity as $\mathbf{T}_G = \mathbf{M}^{-1}\mathbf{T}$, where \mathbf{M} is

$$\mathbf{M} = [\mathbf{I} - (\mathbf{S} - \mathbf{I})\mathbf{G}] \quad (22)$$

and the gradient of the transmission matrix is computed as

$$\begin{aligned} \frac{\partial \mathbf{T}_G}{\partial x_i} &= \frac{\partial \mathbf{M}^{-1}}{\partial x_i} \mathbf{T} = -\mathbf{M}^{-1} \frac{\partial \mathbf{M}}{\partial x_i} \mathbf{M}^{-1} \mathbf{T} \\ &= -\mathbf{M}^{-1} \left[-(\mathbf{S} - \mathbf{I}) \frac{\partial \mathbf{G}}{\partial x_i} \right] \mathbf{M}^{-1} \mathbf{T}. \end{aligned} \quad (23)$$

The expression of the general translation matrix, \mathbf{G} , defined in (8) and which needs to be derived in (23) is provided in [11]. The particularization of the translation matrix between antennas j and k for planar arrays located as shown in Fig. 3 on the xy plane, and with elements without rotation, is expressed as

$$\mathbf{G}_{jk} = \left[\mathbf{R}_k(\phi_{kj}) \mathbf{D}_k \left(\frac{\pi}{2} \right) \mathbf{C} \left(\frac{d}{\lambda} \right) \mathbf{D}_j \left(-\frac{\pi}{2} \right) \mathbf{R}_j(-\phi_{kj}) \right]^T \quad (24)$$

where d and ϕ_{kj} are the distance between the antennas and the angle formed between a line joining them and a reference line, respectively. The matrices \mathbf{R}_k , \mathbf{D}_k , and \mathbf{C} contain the exponential function that relates the φ -dependence of spherical modes, the rotation coefficient and the axial translation coefficient, respectively, as detailed in [27].

The gradient of \mathbf{G}_{jk} is then computed from (24) as

$$\begin{aligned} & \frac{\partial \mathbf{G}_{jk}}{\partial x_k} \\ &= \left[\frac{\partial \mathbf{R}_k(\phi_{kj})}{\partial \phi_{kj}} \frac{\partial \phi_{kj}}{\partial x_k} \mathbf{D}_k \left(\frac{\pi}{2} \right) \mathbf{C} \left(\frac{d}{\lambda} \right) \mathbf{D}_j \left(-\frac{\pi}{2} \right) \mathbf{R}_j(-\phi_{kj}) \right]^T \\ &+ \left[\mathbf{R}_k(\phi_{kj}) \mathbf{D}_k \left(\frac{\pi}{2} \right) \frac{\partial \mathbf{C} \left(\frac{d}{\lambda} \right)}{\partial d} \frac{\partial d}{\partial x_k} \mathbf{D}_j \left(-\frac{\pi}{2} \right) \mathbf{R}_j(-\phi_{kj}) \right]^T \\ &+ \left[\mathbf{R}_k(\phi_{kj}) \mathbf{D}_k \left(\frac{\pi}{2} \right) \mathbf{C} \left(\frac{d}{\lambda} \right) \mathbf{D}_j \left(-\frac{\pi}{2} \right) \frac{\partial \mathbf{R}_j(-\phi_{kj})}{\partial \phi_{kj}} \frac{\partial \phi_{kj}}{\partial x_k} \right]^T. \end{aligned} \quad (25)$$

The derivative with respect to the y -coordinate is computed following the same procedure. In the case of linear arrays, the expression (25) can be simplified because ϕ_{kj} is 0° or 180° depending on the relative position between the antennas. It then reads

$$\frac{\partial \mathbf{G}_{jk}}{\partial x_k} = \left[\mathbf{R}_k(\phi_{kj}) \mathbf{D}_k \left(\frac{\pi}{2} \right) \frac{\partial \mathbf{C} \left(\frac{d}{\lambda} \right)}{\partial d} \frac{\partial d}{\partial x_k} \mathbf{D}_j \left(-\frac{\pi}{2} \right) \mathbf{R}_j(-\phi_{kj}) \right]^T. \quad (26)$$

Although just translations are considered, the rotation matrices \mathbf{R}_k and \mathbf{R}_j also need to be considered. This is because the translation is performed as a combination of rotation-axial translation-rotation, which has been proven to be computationally more efficient in [29]. The gradient of the elements of matrix \mathbf{C} are computed easily using the properties of the derivatives of the spherical Hankel functions of the first and second kinds, and the gradients of the elements of matrix \mathbf{R}_k are computed straightforwardly as they are composed of exponential functions [27].

Following the steps presented in this section, the gradient of the proposed cost function is obtained. The cost function—in which the radiated field is expressed as spherical wave expansions—takes the mutual coupling between elements into account in a rigorous way. In this way, the gradient is obtained and solved very efficiently. At each iteration, one obtains the general transmission matrix (8) and its derivatives (25) versus each element position. These are the most time consuming computations of the method but, as they are obtained analytically, each computation is performed very efficiently. The array characterization comprises the full-wave analysis of the array element and the computation of the radiated field of the array by means of the spherical wave expansion. The FEM simulation of the isolated element, which has to be performed only once, takes about 20 s. The characterization of the array from the GSM of the isolated element is obtained in a less than a second for linear arrays to 30–40 s for planar arrays comprising up to 100 elements. The synthesis of a linear array of 10 to 20 elements can be performed between less than 1 and 3 min on a personal laptop. Larger linear arrays of 50 elements can be synthesized in 15 to 20 min, while planar arrays between 20 and 60 elements will be optimized within 1 to 6 h.

IV. NUMERICAL RESULTS

In order to validate and demonstrate the capabilities of the present method, some linear and planar arrays will be

TABLE I

STEP (δ), FINAL CF (CF_f), NUMBER OF ITERATIONS (ITER.), TIME IN THE ANALYSIS AND SYNTHESIS PROCESS (TIME), AND FINAL SLL (SLL_f)

δ	CF_f	Iter.	Time (s)	SLL_f (dB)
$\lambda_0/20$	0.94	13	52	-14.2
$\lambda_0/30$	0.69	15	60	-14.8
$\lambda_0/50$	0.66	17	68	-15.4
$\lambda_0/80$	0.64	32	130	-15.4

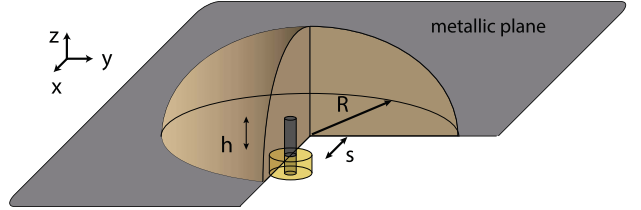


Fig. 4. Geometry of a cylindrical dielectric resonator antenna used as array element: $R = 12.7$, $s = 6.4$, and $h = 6.5$ mm with $\epsilon_r = 9.5$. Coaxial probe feed (50Ω): $r_i = 0.5$ and $r_o = 1.05$ mm with $\epsilon_{rx} = 1.74$.

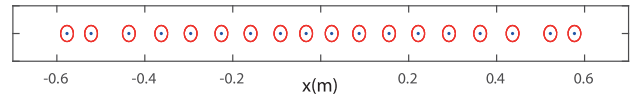


Fig. 5. Synthesized positions of the 18 HDRAs represented with blue dots. The red circles stand for the hemispheres in which the resonators are enclosed.

synthesized using different initial distributions, array specifications, weighting functions, and array elements.

A. Linear Array of Hemispherical Dielectric Resonator Antennas

In this example, an E -plane linear array of 18 hemispherical dielectric resonator antennas (HDRAs) is synthesized, over a maximum length of $14\lambda_0$ at the resonance frequency of 3.64 GHz. The geometry of the array radiator, obtained from [30], is detailed in Fig. 4. The array is designed with a mainbeam width of $R_i = 0.06$ and the weighting function used in this example is [25]

$$W(\hat{u}) = \frac{1}{2} \left[1 - \sin \left(\frac{(\beta - \frac{1+R_i}{2})\pi}{1 - R_i} \right) \right] \frac{1}{\beta^q}. \quad (27)$$

The variable β is the norm of the vector (u_x, u_y) defined as $\beta = \|u_x, u_y\|$, and q allows a softer or sharper variation of W . For this example, $q = 0.5$ and $p = 2$ have been selected. This function gives more importance to the secondary lobes that are close to the mainbeam and it has demonstrated to be the best weighting function for this design. A study has been carried out considering different increment steps, δ , obtaining the results detailed in Table I. As previously mentioned, large values of δ will provide faster convergence but they can fail in obtaining the lowest possible value of the cost function. Small values of δ lead to slower convergence but their accuracy will be higher. For this case, a $\delta = \lambda_0/50$ has been found to be the best possible step value.

The classical density taper technique in [17] is employed as a starting point. In order to emphasize the importance of the electromagnetic analysis in the synthesis process, this synthesis is carried out in two situations. In the first case,

TABLE II
SYNTHESIZED POSITIONS OF THE HDRAs IN EXAMPLE IV.A

No. elem.	1	2	3	4	5	6	7	8	9
Pos. (cm)	-57.69	-52.22	-43.63	-36.26	-29.57	-22.58	-15.96	-9.15	-3.31
No. elem.	10	11	12	13	14	15	16	17	18
Pos. (cm)	2.49	8.74	15.54	22.17	29.16	36.26	43.63	52.22	57.69

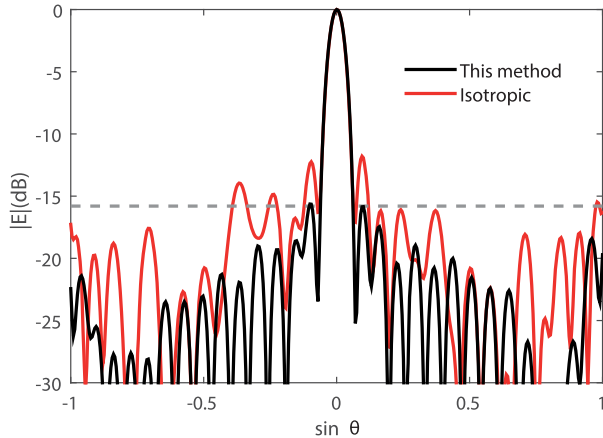


Fig. 6. Radiation pattern of an 18-element HDRa linear array in E -plane with optimized positions obtained from realistic HDRAs (black line) and from isotropic elements (red line). The dashed gray line stands for the maximum SLL obtained in the first case.

the proposed method is used to synthesize the coupled array, and in the second case, the same synthesis method is applied considering isotropic elements. The optimized positions in the first case are detailed in Table II and represented in Fig. 5. The result of the synthesis in both the cases is used to distribute real coupled arrays of HDRAs. The resulting radiation patterns obtained with full-wave simulations are compared in Fig. 6. As can be observed, the simplification in the case of the synthesis with isotropic sources leads to unwanted results with an SLL higher by about 4 dB. This highlights the importance of including mutual coupling. The cross-polar component of the field is negligible in all considered cases.

B. Linear Array of Truncated Tetrahedral Dielectric Resonator Antennas

It is well known that the bandwidth of a periodic array is inversely proportional to the array size [31, Ch. 8, Sec. 3]. Indeed, it is difficult to preserve some array characteristics, such as the SLL, over a large bandwidth. The arbitrary distribution of the elements makes the proposed method suitable for synthesizing wideband arrays. To synthesize the array over a wide frequency band, the cost functions analyzed at different frequencies are combined with an emphasis on the upper and lower frequencies of the desired band. This leads to a multiplication of the number of points in the cost function by the number of frequencies considered.

The element that composes the array is the wideband truncated tetrahedral dielectric resonator antenna (TDRA), obtained from [32], and represented in Fig. 7. It has been designed to operate between 2 and 3 GHz. The array is designed to work with a 26% bandwidth (from 2 to 2.6 GHz). The specifications of the array comprise a linear configuration

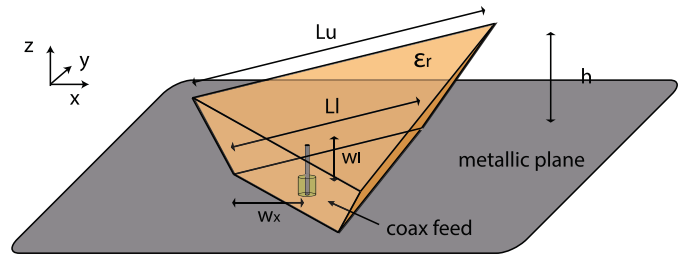


Fig. 7. Geometry of the truncated TDRA used as array element: $h = 2.4$ cm, $L_u = 6.4$, and $L_l = 2.5$ cm with $\epsilon_r = 12$. The feed properties are $w_x = 0.55$ mm and $w_l = 1.15$ mm. Coaxial probe feed (50Ω): $r_i = 0.5$ mm, $r_o = 1.51$ mm, and $\epsilon_{rx} = 1.73$.

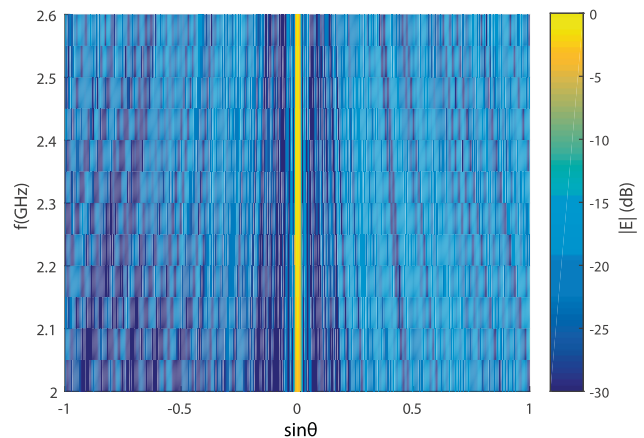


Fig. 8. Synthesized field radiation patterns versus frequency, in steps of 50 MHz, of the 40-element linear array of truncated TDRA along the E -plane.

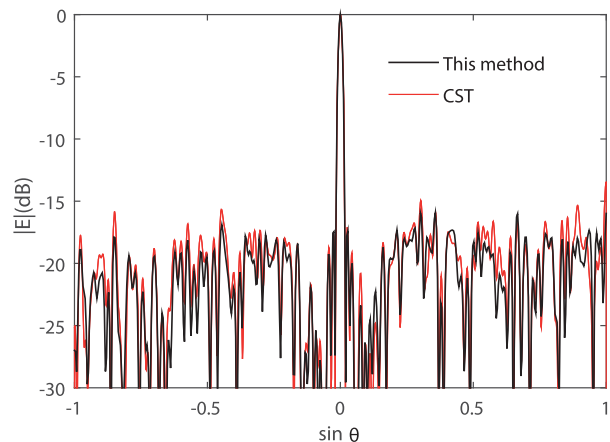


Fig. 9. Field radiation patterns at 2.45 GHz of the 40-element linear array of truncated TDRA along the E -plane with optimized positions obtained with the proposed method. The resulting pattern is compared with the obtained from the commercial software CST.

of 40 elements along the E -plane, distributed over a maximum length of $60\lambda_0$ at its central frequency. For this synthesis, a uniform weighting function has been selected, for angles larger than $R_i = 0.03$. The synthesis process is

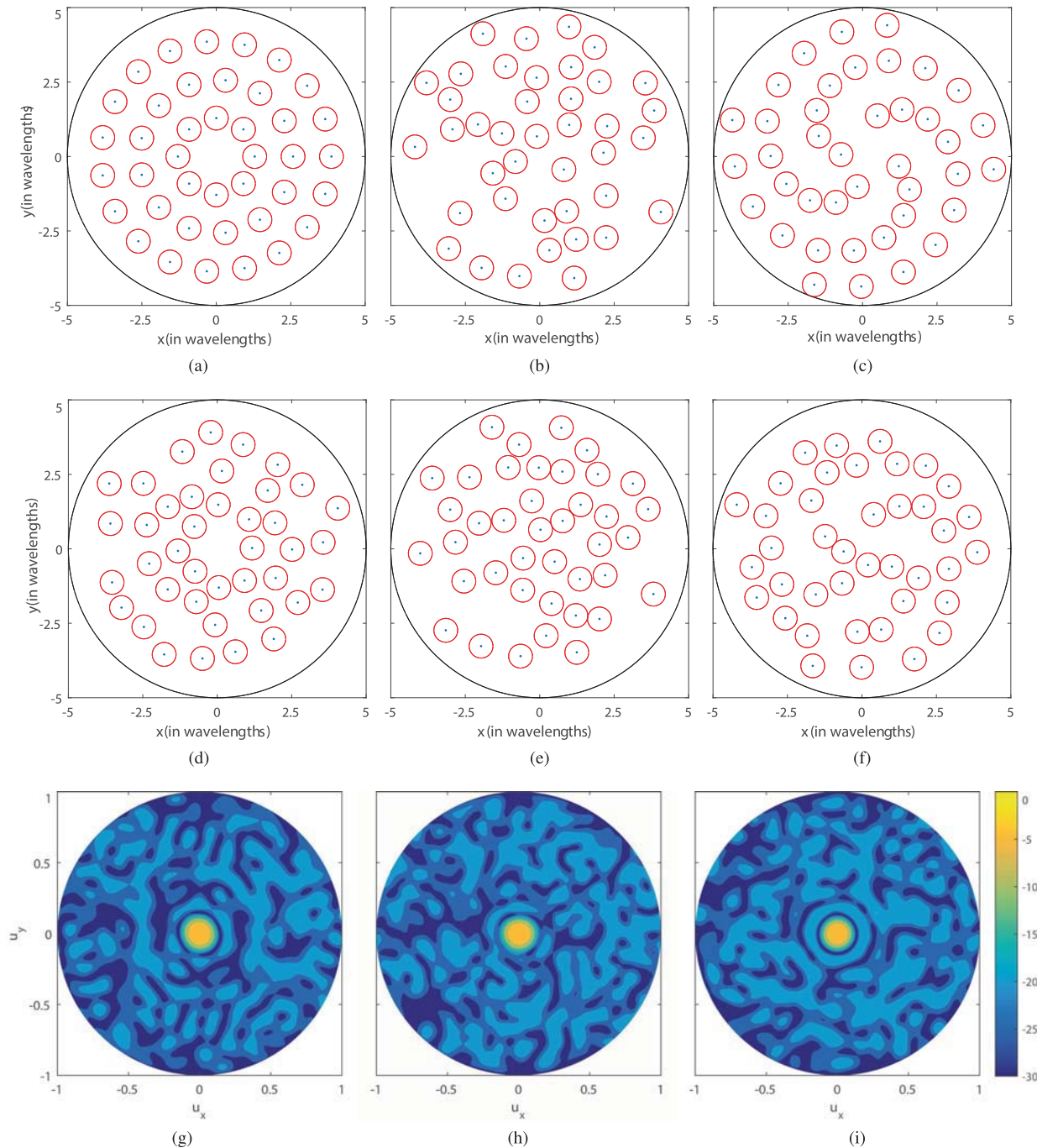


Fig. 10. (a)–(c) Initial configurations considered for the synthesis of a 40-element planar array of truncated TDRAs: circular, random, and sunflower distributions, respectively. (d)–(f) Synthesized distributions obtained with the present method. (g)–(i) Color map representation of the synthesized field radiation patterns at 2.5 GHz for the three different initial configurations and weighting functions.

carried out computing the cost function for three different frequencies: 2, 2.3, and 2.6 GHz. The initial positions are obtained with the classical density taper technique [17] with a maximum SLL of -9 dB. The result of the synthesis is represented in Fig. 8 where one can observe the radiated field over the complete frequency band, with steps of 50 MHz, obtaining an SLL lower than -14.5 dB for every frequency and angle.

For validation purposes, a comparison with the CST Microwave Studio commercial software has been carried out with the elements placed with the distribution obtained in the

synthesis process. The complete array has been analyzed at once with CST at the frequency of 2.45 GHz. In Fig. 9, the radiation pattern obtained with the presented method and with CST are compared. A very good agreement is observed between both simulation results.

C. Planar Array of Tetrahedral Dielectric Resonator Antennas

In the following example, the tetrahedral resonator antenna represented in Fig. 7, used in the previous example, is also employed. In this case, the planar array comprises 40 elements

TABLE III
INITIAL COST FUNCTION (CF_i), FINAL CF (CF_f), INITIAL SLL (SLL_i),
FINAL SLL (SLL_f), NUMBER OF ITERATIONS (IT.), AND TIME IN THE
ANALYSIS AND SYNTHESIS PROCESS (Ti.)

Example	CF_i	CF_f	SLL_i (dB)	SLL_f (dB)	It.	Ti.(min)
Circular	4.70	2.01	-7.3	-16.1	30	125.6
Random	8.83	4.32	-7.2	-15.5	22	82.8
Sunflower	8.4	3.9	-10.24	-15.0	26	100.1

placed in a disk of radius $5\lambda_0$ at a frequency of 2.5 GHz. The desired radiation pattern is a mainlobe at broadside direction, with a beamwidth defined by $R_i = 0.125$. For this example, different initial configurations and weighting functions have been selected looking for the best possible configuration. The initial distributions considered in this example are: the circular distribution [Fig. 10(a)], a random distribution [Fig. 10(b)], and the sunflower distribution [28] [Fig. 10(c)]. In those representations, the black circle stands for the radius delimiting the array surface, the blue dots stand for the exact position of each antenna while the red circles stand for the minimum separation between elements that is fixed in the design process. The SLL obtained with the circular, the random, and the sunflower initial distributions is -7.3 , -7.2 , and -10.24 dB, respectively. Each initial distribution has been synthesized with three different weighting functions: the function expressed in (27) and represented in Fig. 1(a), a slight modification of this one represented in Fig. 1(b)

$$W(\hat{u}) = \frac{1}{2} \left| 1 + \cos^q \left(\left(\beta + \beta_0 - \frac{1}{2} \right) \pi \right) \right| \quad (28)$$

where a focus on the region of secondary lobes centered at β_0 is performed, and a uniform distribution, represented in Fig. 1(c). In (28), $\beta_0 = 0.6$ is used following a previous study for selecting the proper weighting function, as commented in Section III-B. A high p has been selected in order to focus on the highest secondary lobes ($p = 8$).

After the optimization process, the original SLLs have been improved in all cases, however, as the method is nonconvex, different solutions have been obtained for the different configurations. For the circular distribution, the best solution has been obtained with the weighting function (27), obtaining an SLL of -16.1 dB. In the case where the random distribution has been selected as a starting point, the best possible solution has been obtained with a uniform weighting function, obtaining an SLL of -15.5 dB. However, for the sunflower distribution, the lowest SLL has been obtained with the weighting function (28), obtaining in this case an SLL of -15.0 dB. The convergence parameters are represented in Table III. The analysis process for each array distribution takes between 6 and 7 s on a personal laptop (*i7* 16-GB RAM). For the synthesis process, $\delta = \lambda_0/50$ has been selected and the convergence was terminated when the improvement became lower than 1%. The final distributions synthesized by the present method are represented in Fig. 10(d)–(f), respectively. The field radiation patterns of the synthesized arrays are represented in Fig. 10(g)–(i). Although the solutions obtained for each initial distribution are different, the maximum difference in SLLs is of 1.1 dB for this example.

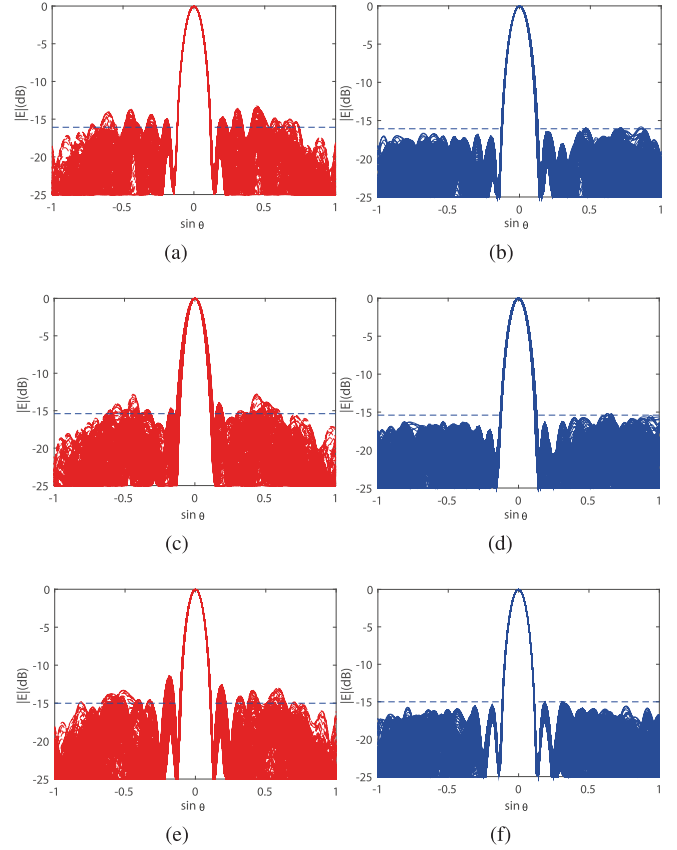


Fig. 11. Comparison between the radiation patterns at 6.1 GHz of a 40-element planar array of truncated TDRA with synthesized positions obtained from isotropic elements (represented in red), and from realistic antennas (in blue). Three initial array configurations are considered. (a) and (b) Circular. (c) and (d) Random. (e) and (f) Sunflower.

The same array synthesis has been carried out considering the elements as isotropic and not taking into account the mutual coupling between them. Fig. 11 (a), (c), and (e) represents the TDRA array radiation patterns, for phi-cuts in step of 1° , with the elements placed with the optimized positions from isotropic sources, for the circular, random, and sunflower initial distributions, respectively. For comparison, Fig. 11 (b), (d), and (f) represents the radiation patterns synthesized from coupled array elements. As observed, the results obtained from the synthesis with isotropic elements have higher secondary lobes that when the present method is used. It is important to notice that the mutual coupling significantly affects the array performance even for cases where the elements are not very close to each other, as in this example where the average distance between elements is larger than one wavelength. The SLL obtained from the circular, random, and sunflower initial distributions with the isotropic synthesis is -13.2 , -12.7 , and -11.3 dB, respectively.

D. Planar Array of Microstrip Patch Antennas

For the last example, the elements are excited with a uniform amplitude distribution and a linear phase taper in order to steer the beam toward a desired direction. The array element is a probe-fed and cavity-backed square microstrip patch antenna, obtained from [11], and detailed in Fig. 12. The array is made up of 100 elements placed in a disk of radius $5\lambda_0$

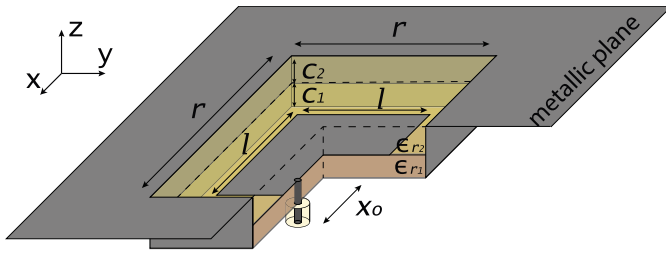


Fig. 12. Geometry of the coaxial probe-fed and cavity-backed square patch antenna used as array element in example IV.C. $l = 1.35$ cm, $r = 1.815$ cm, $c_1 = 2.42$ mm, $c_2 = 2.9$ mm, $x_0 = 1.7$ mm, $\epsilon_{r1} = 2.62$, and $\epsilon_{r2} = 1.0$. Coaxial feed (SubMiniature Version A connector): $\epsilon_{rx} = 1.951$, $r_{in} = 0.65$ mm, and $r_{out} = 2.05$ mm.

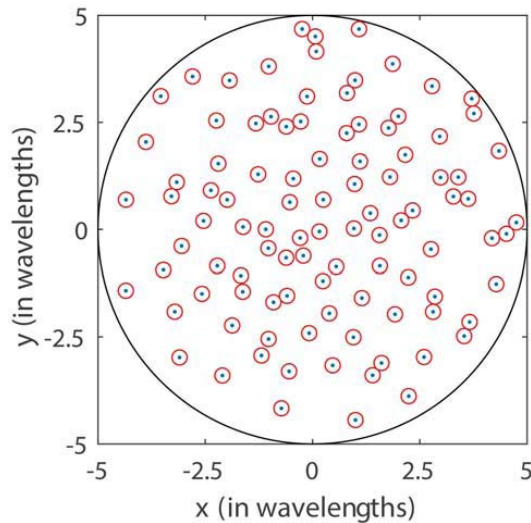


Fig. 13. Synthesized positions of the 100 patch elements placed in a disk of radius $5\lambda_0$ at the resonant frequency of 6.1 GHz.

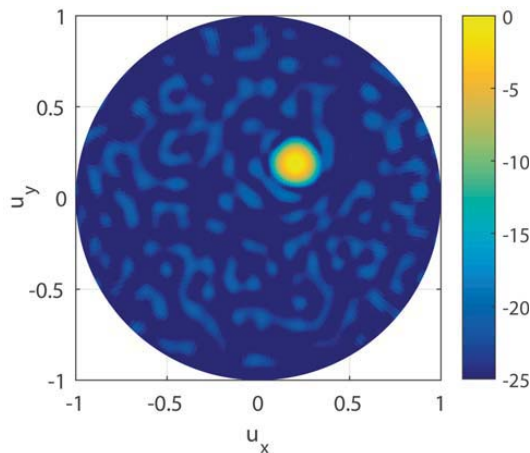


Fig. 14. Synthesized field radiation pattern at 6.1 GHz of a 100-element planar array of cavity-backed microstrip antennas scanned at $u_{x0} = 0.18$ and $u_{y0} = 0.17$.

at the resonant frequency of 6.1 GHz. A phase shift is obtained with the classical theory using the array factor for scanning the array toward $u_{x0} = 0.18$ and $u_{y0} = 0.17$. At each iteration, an excitation phase is assigned to every element depending on its position \mathbf{u}_i according to $\phi = k\hat{\mathbf{u}}_0 \cdot \mathbf{u}_i$. The elements positions are optimized to achieve a beamwidth defined by $R_i = 0.165$ while minimizing the average SLL. The starting

point used in this example is the isotropic synthesis proposed in [25] obtaining an SLL of -16.4 dB. The computational cost per iteration is increased in this example due to the high number of elements. It requires around 4 h per iteration. In this case, $\beta = ||u_x - u_{x0}, u_y - u_{y0}||$ and a uniform weighting function is employed. In Fig. 13, the synthesized positions obtained with the present method are detailed. Fig. 14 represents the field radiation pattern synthesized with the present method, obtaining within five iterations a maximum SLL of -19.7 dB, with a step value of $\delta = \lambda_0/40$.

V. CONCLUSION

In this paper, a new synthesis method for sparse arrays has been presented, where the elements and the mutual coupling between them have been rigorously characterized. Finite elements are used at the element level and spherical waves are used to describe the mutual coupling. A wide variety of radiators can be analyzed with the present method, such as cavity-backed antennas, dielectric resonators, horns, apertures, planar inverted-F antennas, or dipoles. The array characterization and the variation of the mutual coupling due to the variation of the position of the elements are computed analytically, through the calculation of the gradient, versus positions, of the appropriate cost function. This makes this method very efficient for small arrays and suitable for accurate optimization of medium-size arrays.

The efficiency of the local method proposed here provides really good results which depends on the starting configuration. It can be employed also to improve the results of global methods available in the literature or to mitigate the unwanted effects that mutual coupling may induce on these methods. Several examples have been presented, where the strengths of the method and the importance of a rigorous analysis of the array, in terms of mutual coupling, have been emphasized.

REFERENCES

- [1] H. Unz, "Linear arrays with arbitrarily distributed elements," *IRE Trans. Antennas Propag.*, vol. 8, no. 2, pp. 222–223, Mar. 1960.
- [2] M. de Vos, A. Gunst, and R. Nijboer, "The LOFAR telescope: System architecture and signal processing," *Proc. IEEE*, vol. 97, no. 8, pp. 1431–1437, Aug. 2009.
- [3] P. E. Dewdney, P. J. Hall, R. T. Schilizzi, and T. J. L. W. Lazio, "The square kilometre array," *Proc. IEEE*, vol. 97, no. 8, pp. 1482–1496, Aug. 2009.
- [4] "Innovative architectures for reducing the number of controls of multiple beam telecommunications antennas," ESA/ESTEC Tender, Eur. Space Agency, Paris, France, Tech. Rep. AO/1-5598/08/NL/ST, 2009.
- [5] C. Luison *et al.*, "Aperiodic arrays for spaceborne SAR applications," *IEEE Trans. Antennas Propag.*, vol. 60, no. 5, pp. 2285–2294, May 2012.
- [6] W. van Cappellen, S. J. Wijnholds, and J. D. Bregman, "Sparse antenna array configurations in large aperture synthesis radio telescopes," in *Proc. 3rd Eur. Radar Conf. (EuRAD)*, Sep. 2006, pp. 76–79.
- [7] P. Angeletti, G. Toso, and G. Ruggerini, "Array antennas with jointly optimized elements positions and dimensions part II: Planar circular arrays," *IEEE Trans. Antennas Propag.*, vol. 62, no. 4, pp. 1627–1639, Apr. 2014.
- [8] A. Abbaspour-Tamijani and K. Sarabandi, "An affordable millimeter-wave beam-steerable antenna using interleaved planar subarrays," *IEEE Trans. Antennas Propag.*, vol. 51, no. 9, pp. 2193–2202, Sep. 2003.

- [9] R. Maaskant, R. Mittra, and A. Tjhuis, "Fast analysis of large antenna arrays using the characteristic basis function method and the adaptive cross approximation algorithm," *IEEE Trans. Antennas Propag.*, vol. 56, no. 11, pp. 3440–3451, Nov. 2008.
- [10] D. Gonzalez-Ovejero and C. Craeye, "Interpolatory macro basis functions analysis of non-periodic arrays," *IEEE Trans. Antennas Propag.*, vol. 59, no. 8, pp. 3117–3122, Aug. 2011.
- [11] J. Rubio, M. A. González, and J. Zapata, "Generalized-scattering-matrix analysis of a class of finite arrays of coupled antennas by using 3-D FEM and spherical mode expansion," *IEEE Trans. Antennas Propag.*, vol. 53, no. 3, pp. 1133–1144, Mar. 2005.
- [12] C. L. Dolph, "A current distribution for broadside arrays which optimizes the relationship between beam width and side-lobe level," *Proc. IRE*, vol. 34, no. 6, pp. 335–348, Jun. 1946.
- [13] R. S. Elliott and G. J. Stern, "A new technique for shaped beam synthesis of equispaced arrays," *IEEE Trans. Antennas Propag.*, vol. 32, no. 10, pp. 1129–1133, Oct. 1984.
- [14] H. Lebreit and S. Boyd, "Antenna array pattern synthesis via convex optimization," *IEEE Trans. Signal Process.*, vol. 45, no. 3, pp. 526–532, Mar. 1997.
- [15] S. Boyd and L. Vandenberghe, *Convex Optimization*. Cambridge, U.K.: Cambridge Univ. Press, 2003.
- [16] D. G. Kurup, M. Himdi, and A. Rydberg, "Synthesis of uniform amplitude unequally spaced antenna arrays using the differential evolution algorithm," *IEEE Trans. Antennas Propag.*, vol. 51, no. 9, pp. 2210–2217, Sep. 2003.
- [17] W. L. Doyle, "On approximating linear array factors," RAND Corp., Santa Monica, CA, USA, Tech. Rep. RM-3530-PR, 1963.
- [18] O. Bucci, M. D'Urso, T. Isernia, P. Angeletti, and G. Toso, "Deterministic synthesis of uniform amplitude sparse arrays via new density taper techniques," *IEEE Trans. Antennas Propag.*, vol. 58, no. 6, pp. 1949–1958, Jun. 2010.
- [19] L. Cen, Z. L. Yu, W. Ser, and W. Cen, "Linear aperiodic array synthesis using an improved genetic algorithm," *IEEE Trans. Antennas Propag.*, vol. 60, no. 2, pp. 895–902, Feb. 2012.
- [20] B. Clerckx, C. Craeye, D. Vanhoenacker-Janvier, and C. Oestges, "Impact of antenna coupling on 2×2 MIMO communications," *IEEE Trans. Veh. Technol.*, vol. 56, no. 3, pp. 1009–1018, May 2007.
- [21] G. Oliveri, F. Caramanica, and A. Massa, "On the impact of mutual coupling effects on the PSL performances of ADS thinned arrays," *Prog. Electromagn. Res.*, vol. 17, pp. 293–308, 2009.
- [22] G. Prisco and M. D'Urso, "Maximally sparse arrays via sequential convex optimizations," *IEEE Antennas Wireless Propag. Lett.*, vol. 11, pp. 192–195, 2012.
- [23] B. Fuchs, A. Skrivervik, and J. R. Mosig, "Synthesis of uniform amplitude focused beam arrays," *IEEE Antennas Wireless Propag. Lett.*, vol. 11, pp. 1178–1181, 2012.
- [24] C. Bencivenni, M. V. Ivashina, R. Maaskant, and J. Wettergren, "Design of maximally sparse antenna arrays in the presence of mutual coupling," *IEEE Antennas Wireless Propag. Lett.*, vol. 14, pp. 159–162, 2015.
- [25] T. Clavier *et al.*, "A global-local synthesis approach for large non-regular arrays," *IEEE Trans. Antennas Propag.*, vol. 62, no. 4, pp. 1596–1606, Apr. 2014.
- [26] J. Rubio, M. A. González, and J. Zapata, "Analysis of cavity-backed microstrip antennas by a 3-D finite element/segmentation method and a matrix Lanczos-Padé algorithm (SFELP)," *IEEE Antennas Wireless Propag. Lett.*, vol. 1, no. 1, pp. 193–195, 2002.
- [27] J. E. Hansen, *Spherical Near-Field Antenna Measurements* (IET Electromagnetic Waves Series). London, U.K.: Peter Peregrinus, Ltd., 1988.
- [28] M. C. Viganó, G. Toso, G. Caille, C. Mangenot, and I. E. Lager, "Sunflower array antenna with adjustable density taper," *Int. J. Antennas Propag.*, vol. 2009, Apr. 2009, Art. no. 624035.
- [29] T. J. Dufva, J. Sarvas, and J. C.-E. Sten, "Unified derivation of the translational addition theorems for the spherical scalar and vector wave functions," *Prog. Electromagn. Res. B*, vol. 4, pp. 79–99, 2008.
- [30] K. W. Leung, K. M. Luk, K. Y. A. Lai, and D. Lin, "Theory and experiment of a coaxial probe fed hemispherical dielectric resonator antenna," *IEEE Trans. Antennas Propag.*, vol. 41, no. 10, pp. 1390–1398, Oct. 1993.
- [31] R. J. Mailloux, *Phased Array Antenna Handbook*. Norwood, MA, USA: Artech House, 2005.
- [32] A. A. Kishk, "Wide-band truncated tetrahedron dielectric resonator antenna excited by a coaxial probe," *IEEE Trans. Antennas Propag.*, vol. 51, no. 10, pp. 2913–2917, Oct. 2003.



J. Ignacio Echeveste was born in Madrid, Spain. He received the Electrical Engineering degree from the Universidad Miguel Hernández de Elche, Alicante, Spain, in 2010, and the M.S. and Ph.D. degrees from the Universidad Politécnica de Madrid (UPM), Madrid, in 2012 and 2016, respectively.

From 2011 to 2016, he was with the Departamento de Señales, Sistemas y Radiocomunicaciones, UPM. He was a visiting Ph.D. student with the Université catholique de Louvain (UCL), Louvain-la-Neuve, Belgium, in 2015. In 2016, he joined the ICTEAM Institute, UCL, as a Post-Doctoral Researcher. His current research interests include numerical methods and optimization techniques applied to the analysis and synthesis of array antennas.



Miguel Á. González de Aza was born in Madrid, Spain. He received the Ingeniero de Telecomunicación and Ph.D. degrees from the Universidad Politécnica de Madrid (UPM), Madrid, in 1989 and 1997, respectively.

Since 1990, he has been with the Escuela Técnica Superior de Ingenieros de Telecomunicación, Universidad Politécnica de Madrid, first as a Research Assistant, as an Assistant Professor from 1992 to 1997 and an Associate Professor in 1997. His current research interests include analytical and numerical techniques for the analysis and design of antennas, arrays of antennas and microwave passive circuits.



Jesús Rubio was born in Talavera de la Reina, Spain, in 1971. He received the Ingeniero de Telecomunicación and Ph.D. degrees from the Universidad Politécnica de Madrid, Madrid, Spain, in 1995 and 1998.

Since 1994, he has been collaborating with the Departamento de Electromagnetismo y Teoría de Circuitos, Universidad Politécnica de Madrid. He is currently as a Professor with the Departamento de Tecnología de los Computadores y de las Comunicaciones, Universidad de Extremadura, Badajoz, Spain. His current research interests include finite-element method and modal analysis to antennas and passive microwave circuits problems.



Christophe Craeye (M'98–SM'11) was born in Belgium in 1971. He received the Electrical Engineering and B.Phil. degrees from the Université catholique de Louvain (UCL), Louvain-la-Neuve, Belgium, and the Ph.D. degree in applied sciences from UCL, in 1994 and 1998, respectively.

From 1994 to 1999, he was a Teaching Assistant with UCL and carried out research on the radar signature of the sea surface perturbed by rain, in collaboration with NASA and ESA. From 1999 to 2001, he was a Post-Doctoral Researcher with the Eindhoven University of Technology, Eindhoven, The Netherlands. He was with the University of Massachusetts, Amherst, MA, USA, in 1999. He was with the Netherlands Institute for Research in Astronomy, Dwingeloo, The Netherlands, in 2001. In 2002, he started an antenna research activity with UCL, where he is currently a Professor. He was with the Astrophysics and Detectors Group, University of Cambridge, Cambridge, U.K., in 2011. His research was funded by the Région Wallonne, European Commission, ESA, FNRS, and UCL. His current research interests include wideband phased arrays devoted to the square kilometer array radio telescope, finite antenna arrays, wideband antennas, small antennas, metamaterials, and numerical methods for fields in periodic media, with applications to communication and sensing systems.

Dr. Craeye received the 2005–2008 Georges Vanderlinden Prize from the Belgian Royal Academy of Sciences, in 2009. He was an Associate Editor of the *IEEE TRANSACTIONS ON ANTENNAS AND PROPAGATION* from 2004 to 2010. He currently serves as an Associate Editor of the *IEEE Antennas and Wireless Propagation Letters*.